



A carbon@SnO₂@MoO₂ nanoarchitectonic derived from cellulose substance as an anodic material for lithium-ion batteries

Dongmei Qi · Sijun Ren · Shun Li · Jianguo Huang

Received: 31 May 2022 / Accepted: 25 July 2022 / Published online: 5 August 2022
© The Author(s), under exclusive licence to Springer Nature B.V. 2022

Abstract A novel cellulose substance (ordinary laboratory filter paper) derived hierarchical carbon/tin-oxide/molybdenum-dioxide (carbon@SnO₂@MoO₂) ternary nanoarchitectonic was fabricated by the self-assembly process and subsequent carbonization treatment. The resultant nanocomposite was composed of thin tin oxide layer sandwiched between the porous carbon nanofibers and the external molybdenum dioxide coating layer, where the thickness of the molybdenum dioxide coating layer was controlled facilely. As being utilized as an anodic material for lithium-ion batteries, the nanocomposite displayed high reversible capacity and good rate performance that are superior to those of the carbon@MoO₂ hybrid without SnO₂. The

good electrochemical performance of the anode was benefited from the sophisticated multi-level structures of the composite, small sizes of the tin oxide (ca. 5 nm) and molybdenum dioxide (ca. 6 nm) nanocrystallites contained therein, and the synergistic interactions between the tin oxide layer, the outer molybdenum dioxide coating layers, as well as the porous carbon buffering matrix. For such a composite with MoO₂ and SnO₂ contents of 20 and 10%, respectively, by weight, it delivered a specific capacity of 608.1 mAh g⁻¹ after 100 discharge/charge cycles at the current rate of 100 mA g⁻¹. The current work presents a facile and cost-effective pathway to synthesize bio-substance derived nanocomposite materials for energy applications.

Supplementary Information The online version contains supplementary material available at <https://doi.org/10.1007/s11051-022-05542-z>.

This article is part of the topical collection: Nanoarchitectonics for Functional Particles and Materials

Guest Editor: Katsuhiko Ariga

D. Qi · S. Ren · S. Li · J. Huang (✉)
Department of Chemistry, Zhejiang University,
Hangzhou 310027, Zhejiang, China
e-mail: jghuang@zju.edu.cn

D. Qi
Analysis Center of Agrobiolgy and Environmental
Sciences, Zhejiang University, Hangzhou 310058, China

Keywords Nanoarchitectonics · Self-assembly · Lithium-ion batteries · Tin oxide · Molybdenum dioxide · Nanocomposites · Energy storage

Introduction

The recent decades have witnessed the rapid and significant developments of rechargeable lithium-ion batteries (LIBs) for their potential applications in various portable electronics and electric vehicles (EVs) as well as hybrid electric vehicles [1, 2]. As one of the most important component of the battery system, electrode materials mostly dominate the battery

performances of LIBs [3]. However, the conventional graphite-based anodes are unable to meet the ever-growing demands for high-performance LIBs [4, 5]; therefore, the research for the next-generation anodic material with low cost, high specific capacity, long cycle life as well as good rate-capability is urgent at present. The construction of various nanoarchitectonics by different chemical processes provides an effective methodology for the development of a large variety of functional nanostructured materials [6–10], in particular, the ones for energy applications [11–14].

Metal oxides have been considered appealing candidates as electrode materials for LIBs, owing to the better operational safety and higher theoretical capacities compared with those of the traditional graphite-based anodic materials [15]. Among the various metal oxides, tin oxide (SnO_2) has been extensively studied due to the high theoretical storage capacity of 782 mAh g^{-1} and low cost, which makes it to be a substitute for graphite-based anode in LIBs [16–18]. However, in practical application, SnO_2 based anodes are typically subjected to the serious volume change upon the repeated lithiation/delithiation processes, resulting in the structural collapse of the active material and ultimately sharp capacity fading and short battery life of the pure SnO_2 electrodes [2, 19]. One of the available approaches to improve the performances is to fabricate the SnO_2 -based composite oxides to introduce the synergistic effects benefited from different components contained in the composite [19].

Among the different metal oxides, molybdenum dioxide (MoO_2) has received tremendous attention due to the high theoretical capacity (838 mAh g^{-1}), less charging potential, and superior metallic electronic conductivity ($> 1 \times 10^4 \text{ S cm}^{-1}$), as well as facile ion transport properties [20, 21]. A number of MoO_2 anodic materials with specific nanostructures, such as nanoparticles [22], nanorods [23], nanosheets [24], as well as core-shell hierarchical microcapsule structures [25], have been reported with improved lithium storage performance for LIBs. In spite of the high initial specific capacity delivered by the nanostructured MoO_2 anodes, the cyclability and rate capability of which are still not satisfactory [26].

To overcome these drawbacks, hybridizing nanoscaled MoO_2 with elastic and conductive carbon species has been proven to be an effective strategy to improve the structural integrity and facilitate lithium-ions (Li-ions) and electrons transport, hence, resulting in the greatly

enhanced cycling stability of the electrodes [27]. In this regard, some MoO_2/C composites have been synthesized and employed as anodic materials for LIBs. For instance, MoO_2 /graphene composites with MoO_2 nanoparticles homogeneously dispersing in the three-dimensional network of the graphene matrixes were fabricated as anodic materials for LIBs by different approaches, such as the layer-by-layer (LbL) assembly method [28], the chemical reduction processes [29], and the microwave-assisted hydrothermal process followed by thermal annealing [30]. And the MoO_2/C composite with MoO_2 nanoparticles anchored uniformly on the carbon nanotubes [31] or carbon nanofibers [32] was fabricated hydrothermally to exhibit improved electrochemical behaviors as compared with the pure MoO_2 counterparts. Besides, hierarchical MoO_2/C spheres were obtained via the ethanol thermal reduction method followed by an annealing process [33] or through the calcination of $\alpha\text{-MoO}_3$ /resin precursor formed by a hydrothermal method [34], displaying high reversible capacities, good rate capability as well as high cycling stability for LIBs. Furthermore, porous MoO_2/C nano-octahedrons were fabricated via the calcination of the polyoxometalate-based metal-organic framework (POMOF) precursor combined with etching treatment, which was used as a high-performance and stable host for Li-ion accommodation [35]. More instances, including MoO_2 /multiwalled carbon nanotubes hybrid [36], MoO_2 /ordered mesoporous carbon composite [26, 37], and cage-like structured MoO_2/C composite [38] were prepared via different approaches, exhibiting enhanced anodic performances for LIBs. While, to the best of our knowledge, the synthesis of a three-dimensional carbon/tin-oxide/molybdenum-dioxide ($\text{carbon@SnO}_2@\text{MoO}_2$) ternary composite as an anodic material for LIBs has not been reported to date. In the current work, a new hierarchically nanofibrous $\text{carbon@SnO}_2@\text{MoO}_2$ nanoarchitectonic was fabricated via a layer-by-layer (LbL) self-assemble approach, utilizing the low-cost natural cellulose substance (ordinary laboratory filter paper) as the structural scaffold and carbon source.

Biomimetic syntheses based on the self-assembly technique are proven to be a highly versatile and effective route to fabricate functional materials with tailored structures and properties [12, 39–44]. As an ideal template or scaffold, natural cellulose substances (i.e., ordinary laboratory filter paper) hold inherently unique hierarchically multi-level porous structures. Furthermore, the abundant hydroxyl and ether groups possessed by

cellulose substances enable them to be modified by various guest species via hydrogen or covalent bonding, thus bringing in specific properties and characters to the artificial matters [45]. When being evaluated as anodic materials for LIBs, the cellulose substance derived metal oxide-based nanomaterials displayed desirable electrochemical performances due to the fantastic bio-inspired morphologies [46–55]. In addition, the carbon nanofiber network originated from the carbonization of the cellulose nanofibers of the filter paper and serves as a carbon matrix to immobilize the metal oxide nanoparticles to form the corresponding composites. Moreover, the hierarchical three-dimensional porous structure of the carbon matrix would relax the drastic volume variation of the active material during the repeated discharge/charge processes, thus leading to enhanced lithium storage properties. The sol–gel and hydrothermal processes are commonly employed to fabricate the cellulose-derived metal oxide-based anodic materials for LIBs by utilizing the corresponding metal alkoxides as the precursors; hence, the materials thus fabricated are restricted to specific oxides such as tin oxide and titania. To break this limitation, adopting specific polyoxometalate clusters as the metal oxide precursors would effectively extend the range of the bio-inspired metal oxide materials that can be obtained. As shown in the current work, a new hierarchical fibrous carbon@SnO₂@MoO₂ nanocomposite was synthesized by a layer-by-layer self-assembly approach using polyoxomolybdate (POM) cluster as the critical building block and natural cellulose substance (*e.g.* filter paper) as the structural scaffold and the carbon source. The resultant nanocomposite is composed of tin oxide thin layer coated carbon nanofibers with molybdenum dioxide nanoparticles immobilized as an external coating layer on the surfaces. When utilized as an anodic material for LIBs, this composite presented an improved reversible specific capacity and good rate performance as compared with the counter material of the carbon@MoO₂ hybrid. This is ascribed to the sophisticated multi-level nanostructural features of the composite, as well as the synergistic interaction between the MoO₂, SnO₂, and carbon components contained therein.

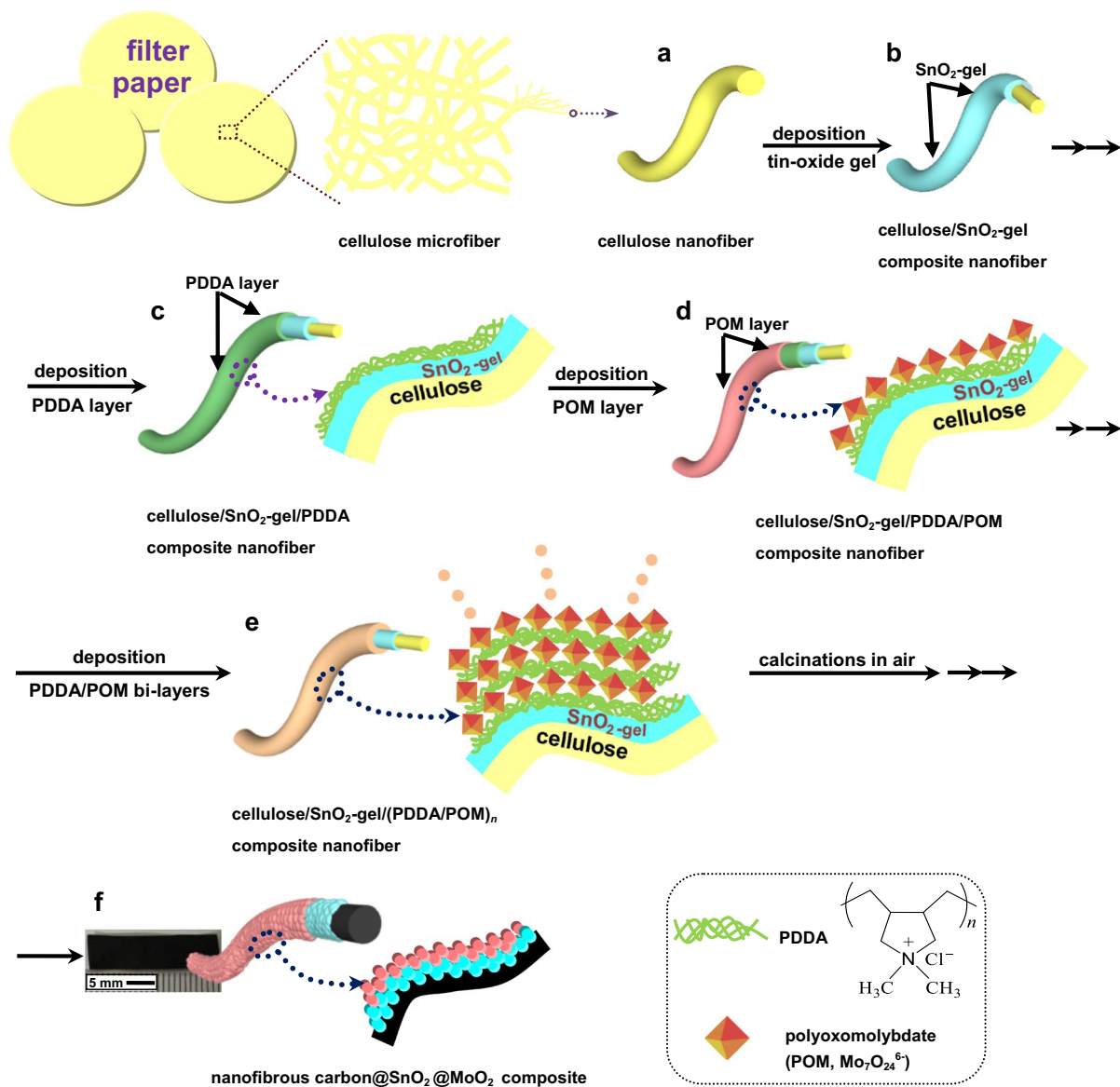
Experimental part

Chemicals

Tin(IV) isopropoxide [(Sn(OⁱPr)₄, 99% metals basis, 10% w/v in isopropanol] was bought from Alfa Aesar. Ammonium molybdate tetrahydrate (AHM) was purchased from J&K Chemical Ltd. And polydiallyldimethylammonium chloride (PDDA, average $M_w < 100,000 - 350,000$, 20 wt% aqueous solutions) was bought from Sigma-Aldrich. All the solvents were guaranteed reagents and used without purification. Commercial quantitative filter paper (ashless, made from cotton) was purchased from Hangzhou Xinhua Paper Industry Co. Ltd. (China). The filter paper is composed of cellulose microfibrils, which are assembled by cellulose nanofibers with diameters varying from tens to hundred nanometers. The water used in all the relevant cases was purified by using a Milli-Q advantage A 10 system (Millipore, Bedford, MA, USA) with resistivity higher than 18.2 MΩ cm.

Fabrication of the nanofibrous carbon@SnO₂@MoO₂ composite

The fabrication process is illustrated in Scheme 1. Firstly, a piece of filter paper ($d = 3.0$ cm) was placed into a glass funnel, and washed by suction filtration of ethanol, then dried by air flow prior to use. Next, ultrathin tin-oxide gel layers were initially deposited to coat the nanofibers of the bulky filter paper through the surface sol–gel process performed at 50 °C, utilizing Sn(OⁱPr)₄ (10 mM in 1:1 v:v methanol/isopropanol) as precursor according to our previous reports (Scheme 1b) [53, 54]. The deposition cycle of the SnO₂-gel layer was repeated 5 times. And the as-prepared cellulose/SnO₂-gel composite sheet was further utilized to immobilize the PDDA/POM electrolyte bilayers driven by the electrostatic interaction. To this end, PDDA solution (20.0 mL, 1.0 mg mL⁻¹ in 0.5 M sodium chloride aqueous solution) was added to the filter funnel, half of which was slowly suction filtered through the cellulose/SnO₂-gel composite sheet. The rest solution remained for 15 min to achieve the adsorption of PDDA onto the SnO₂-gel surface. After that, the remaining solution was suction-filtered, and the as-deposited composite sheet was rinsed immediately by suction-filtration of sodium chloride aqueous solution (60.0 mL) and water (60.0 mL) to get rid of



Scheme 1 Schematic illustration of the synthetic route of the nanofibrous carbon@SnO₂@MoO₂ composite derived from the natural cellulose matter (ordinary laboratory filter paper). **a** An individual cellulose nanofiber of initial filter paper; **b** thin tin oxide-gel layer was deposited to coat the cellulose nanofibers via the surface sol–gel process, yielding the cellulose/SnO₂-gel composite; **c** coating a positively charged PDDA layer onto the surface of cellulose/SnO₂-gel nanofibers to obtain the cellulose/SnO₂-gel/PDDA composite; **d** deposit-

ing a negatively charged POM cluster layer onto the resultant composite fiber surfaces to produce the cellulose/SnO₂-gel/PDDA/POM composite; **e** alternative deposition of the PDDA/POM bilayers onto the nanofiber surface to result in the cellulose/SnO₂-gel/(PDDA/POM)_n composite; **f** carbonizing the cellulose/SnO₂-gel/(PDDA/POM)_n composite sheet in Ar atmosphere to give the hierarchical carbon@SnO₂@MoO₂ nanofibrous composite, the inset exhibits the photograph of the corresponding bulk sample

the excess reagent, resulting in the cellulose/SnO₂-gel/PDDA composite fiber (Scheme 1c). The resultant composite sheet was dried by airflow, and afterward, 20.0 mL AHM aqueous solution (0.05 M) was

used as the precursor to similarly deposited the negatively charged POM layer onto the composite fiber surface to form the cellulose/SnO₂-gel/PDDA/POM composite (Scheme 1d). The deposition cycles of the

PDDA/POM bilayer were repeated n times, and each cellulose nanofiber of the filter paper was coated by $\text{SnO}_2\text{-gel}/(\text{PDDA}/\text{POM})_n$ composite films as shown in Scheme 1e. Eventually, the as-obtained cellulose/ $\text{SnO}_2\text{-gel}/(\text{PDDA}/\text{POM})_n$ composite sheet was carbonized under the Ar atmosphere at 500 °C for 6 h (heating rate of 2 °C min^{-1}) to remove the PDDA component, and meanwhile, the cellulose, amorphous $\text{SnO}_2\text{-gel}$, and POM cluster layer were converted into the amorphous carbon, rutile SnO_2 , and monoclinic MoO_2 phase, respectively, thus yielding the carbon@ SnO_2 @ MoO_2 nanocomposite with hierarchical nanofibrous structures (Scheme 1f). As for the control carbon@ MoO_2 material, it was prepared by the impregnation method followed by a similar carbonization treatment. Briefly, one piece of filter paper ($d=3.0$ cm) was immersed in a 0.05 M AHM solution for 12 h to achieve the adsorption balance of the POM cluster onto the cellulose fiber surfaces. Then the sample was fetched from the solution and dried at room temperature, followed by the same carbonization treatment mentioned above to generate the carbon@ MoO_2 composite.

Characterizations

X-ray powder diffraction (XRD) patterns were measured on a Philips X'Pert PRO diffractometer with a Cu K_α radiation source ($\lambda=0.15405$ nm) between 10 and 80°. Raman spectra were conducted on a Jobin Yvon LabRAM HR UV Raman spectrometer with an excitation wavelength of 532 nm under ambient conditions. Thermogravimetric (TG) analyses were carried out on a NETZSCH STA 409 PC/PG thermal analyzer and tested from room temperature to 800 °C with a heating rate of 10 °C min^{-1} in airflow. The specimens for electron microscopic measurements were made by sonicating a small amount of the relevant sample (*ca.* 0.5 mg) in ethanol (1.0 mL) to obtain a suspension, and drops of which were placed onto a piece of aluminum foil for the field-emission electron microscopy (FE-SEM) observations or a carbon-coated copper grid for the transmission electron microscopy (TEM) observations. All the specimens were dried in the air before the measurements. FE-SEM images were acquired on a Hitachi SU-70 electron microscope equipped with EDSX HORIBA X-Max80006 apparatus working at an accelerating voltage of 25.0 kV, and the specimens were sputtered

with platinum to alleviate charging effects during the examinations. TEM and HR-TEM micrographs were obtained using a Hitachi HT-7700 microscope working at an accelerating voltage of 100 kV and a Philips FEI Tecnai G2F30 S-Twin microscope working at an accelerating voltage of 200 kV, respectively. X-ray photoelectron spectroscopy (XPS) measurements were performed on a VG ESCALAB MkII spectrophotometer with a monochromatic and focused Mg K_α X-ray source at the energy of 1253.6 eV, and all of the binding energies were internally referenced to the C1s peak at 284.5 eV. Nitrogen adsorption–desorption isotherms were collected by using a Micromeritics ASAP 2020 analyzer at -196 °C; the specific surface areas were calculated based on the Brunauer–Emmett–Teller (BET) model over the relative pressure range of 0.05–0.30, and the pore volume was determined via the Barrett–Joyner–Halenda (BJH) approach by integration of the pore size distributions in the range of 1.7–300 nm.

Electrochemical measurements

Standard CR2025 type coin cells were assembled to evaluate the electrochemical properties of the nanofibrous carbon@ SnO_2 @ MoO_2 composites and the comparative carbon@ MoO_2 hybrid. The working electrodes were constructed by mixing the active material, conductive acetylene black carbon, and polyvinylidene fluoride (PVDF) in a weight ratio of 70:20:10 in N-methyl-pyrrolidinone (NMP) to form a uniform slurry, which was further spread onto a copper foam substrate (as a current collector). The coated electrode was dried at 80 °C for 24 h in a vacuum oven to remove the solvent and then pressed at a pressure of 10 atm. The active material mass coated on each electrode was 2.15 mg cm^{-2} . Then the coin cells were assembled in an argon-filled glove box where both the oxygen and moisture levels were below 0.1 ppm. Lithium foil was utilized as the counter electrode, and polypropylene film (Celgard-2300) was employed as the separator to isolate the two electrodes. The electrolyte was made of lithium hexafluorophosphate (LiPF_6 , 1.0 M) dissolved in a mixture of ethylene carbonate (EC) and dimethyl carbonate (DMC) with a volume ration of 1:1, and about 50 μL of which was used for fabricating each electrode. Cyclic voltammetry (CV) curves were recorded on a CHI760D electrochemical workstation (CH

Instruments, Inc., China) at a scan rate of 0.2 mV s^{-1} in the potential range of $0.01 - 3.0 \text{ V vs. Li/Li}^+$. The battery performance was determined at room temperature by using a Neware battery testing system (Neware Technology Co., Ltd, Shenzhen, China). The galvanostatic charge/discharge capacities were tested by cycling the half-cells at a different current rate between 0.01 and 3.0 V ; the specific capacities were calculated according to the total mass of the active materials. To investigate the structural change of the composite electrode after 100 discharge/charge cycles, the cells were disassembled, and the working electrode was rinsed in acetone for 10 min to get rid of the remained electrolyte and dried prior to electron microscopic analyses.

Results and discussions

Structural characterization of the carbon@SnO₂@MoO₂ composite

As illustrated in Scheme 1, to obtain the cellulose substance derived nanofibrous carbon@SnO₂@MoO₂ composite, ultrathin SnO₂-gel was firstly deposited to coat the cellulose nanofibers of the filter paper through a surface sol-gel process, utilizing tin (IV) isopropoxide as a precursor. Afterward, the PDDA/POM double layers were alternatively deposited onto the resultant cellulose/SnO₂-gel composite fiber surfaces followed by carbonization treatment. The resultant carbon@SnO₂@MoO₂ composite is composed of SnO₂ thin layer coated carbon nanofibers with MoO₂ nanoparticles anchored as an external coating layer on the surfaces. In order to adjust the MoO₂ content in the final carbon@SnO₂@MoO₂ composites, the deposition cycle of the PDDA/POM double layers was repeated 5, 10, and 15 times, respectively, and the resultant MoO₂ content contained in the samples was determined to be 4, 12, and 20 wt.%, respectively, based on the energy-dispersive X-ray spectroscopy (EDS) results (Fig. S1a–c) as well as the thermogravimetric (TG) analyses (Fig. S1d). And the corresponding samples are accordingly marked as carbon–13%/SnO₂–4%/MoO₂, carbon–13%/SnO₂–12%/MoO₂, and carbon–10%/SnO₂–20%/MoO₂, respectively. As for the control sample carbon@MoO₂ composite prepared by an impregnation method combined with the same carbonization

treatment, the MoO₂ content is measured to be 23% on the basis of TG analyses, thus the relevant sample is denoted as carbon–23%/MoO₂ (Fig. S2a).

Figure 1a shows the XRD diffraction patterns of the nanofibrous carbon@SnO₂@MoO₂ composites with varied MoO₂ contents. For the sample carbon–13%/SnO₂–4%/MoO₂, two series of diffraction peaks are observed. The ones at $2\theta = 26.6, 34.0, 51.8,$ and 65.9° are assigned to the (110), (101), (211), and (301) planes of tetragonal rutile-structured SnO₂ (JCPDS no.41–1445), respectively, which agrees well with the XRD result of the carbon@SnO₂ sample reported in our previous work [53]; and those at $26.0, 36.5, 53.5,$ and 66.6° are indexed to the (–111), (200), (–312), and (–402) planes of the monoclinic MoO₂ phase (JCPDS no.32–0671) [56], respectively. It is noteworthy that the diffraction peaks related to the monoclinic MoO₂ phase become distinct with

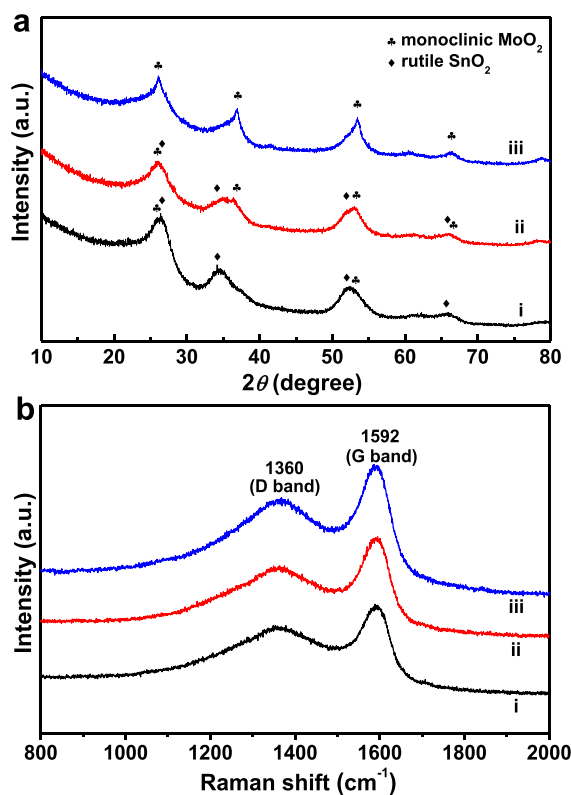


Fig. 1 Powder X-ray diffraction patterns (a) and Raman spectra (b) of the commercial filter paper-derived carbon@SnO₂@MoO₂ nanocomposites (i. carbon–13%/SnO₂–4%/MoO₂, ii. carbon–13%/SnO₂–12%/MoO₂, and iii. carbon–10%/SnO₂–20%/MoO₂)

the increment of the MoO₂ contents in the carbon@SnO₂@MoO₂ composites, and when the MoO₂ content is up to 20 wt.%, only typical diffraction peaks of monoclinic MoO₂ phase are detected, due to the relatively thick MoO₂ coating layer on the composite fiber surface. Moreover, no other diffraction peak related to metallic Sn or MoO₃ is found, indicating the formation of MoO₂ was achieved by the carbothermal reduction, and meanwhile, SnO₂ did not transform into Sn in this process. As for the control carbon–23%/MoO₂ composite, except for the series of weak reflection planes belonging to the monoclinic-structured MoO₂, another prominent broad peak is observed at *ca.* 24.5°, which is attributed to the amorphous carbon contained in this sample (Fig. S2b).

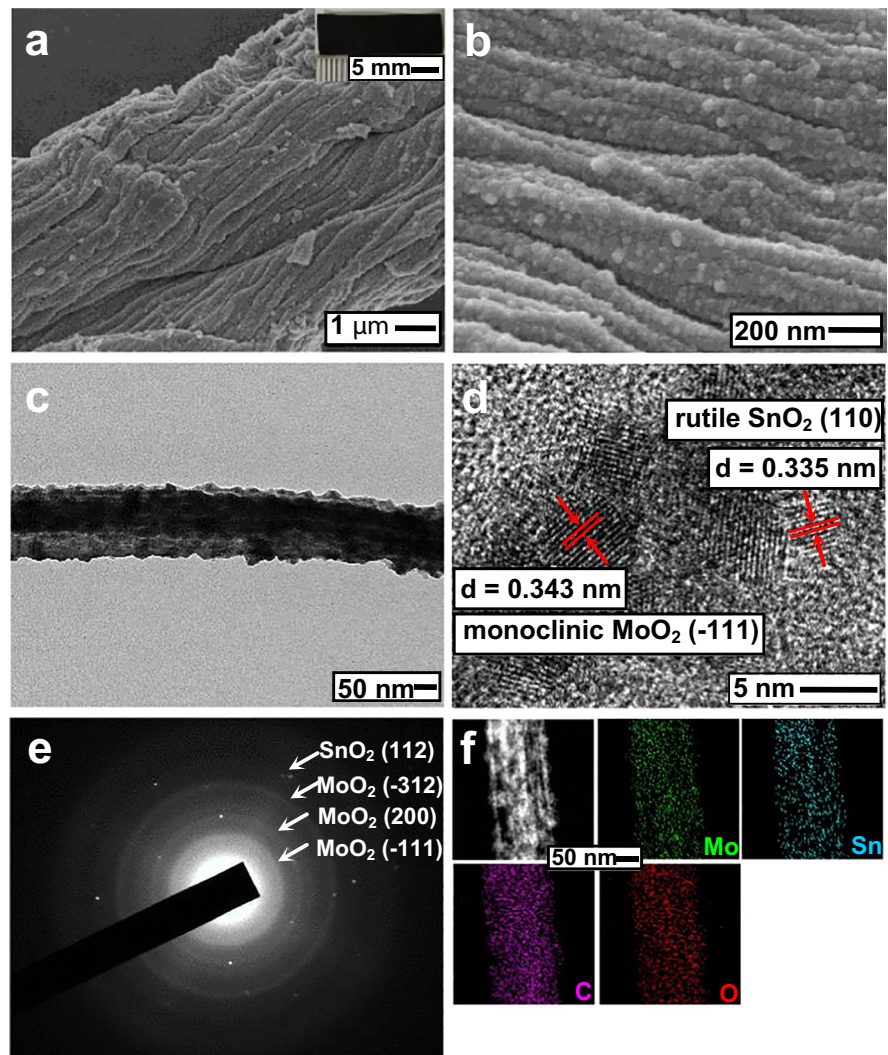
Figure 1b exhibits the Raman spectra of the nanofibrous carbon@SnO₂@MoO₂ composites derived from natural cellulose substances. It is observed that all the Raman spectra of the samples displayed two typical peaks of carbon species, which are a weak *D*-band at *ca.* 1360 cm⁻¹ and a strong *G*-band at *ca.* 1592 cm⁻¹, corresponding to the defect-induced disordered structures of carbon and the in-plane carbon–carbon stretching vibrations [57–59], respectively. The *I_G/I_D* value of all the nanocomposites was calculated to be about 1.20. For the control sample carbon–23%/MoO₂ (Fig. S2c), similar Raman signals of carbon were detected, and the *I_G/I_D* ratio was 1.33. The lower *I_G/I_D* value of the carbon@SnO₂@MoO₂ composites indicates a more disordered carbon structure contained in this composite, which is due to the distribution of the SnO₂ and MoO₂ nanoparticles on the surfaces of the carbon nanofibers, resulting in more lattice defects of the carbon. These results reveal that the carbon species contained in these nanocomposites are relatively disordered in the structure, which is in good accordance with the XRD examinations.

Template-based LbL self-assemble approach is well known as a facile and effective bottom-up strategy for the fabrication of functional nanomaterials as replicas of the initial template substances [60]. As demonstrated by the electron micrographs in Fig. 2, the current nanofibrous carbon–10%/SnO₂–20%/MoO₂ composite appears to be a bulky black sheet (Fig. 2a, inset), which contains a hierarchical microfiber structure, and each microfiber is composed of assemblies of three-dimensionally cross-linked nanofibers with the external diameters

varied from ten to hundreds of nanometers (Fig. 2a). This unique, hierarchically multi-level morphology was obviously inherited from the original cellulose scaffold. And a high-magnification SEM image displayed in Fig. 2b shows the nanofibers are coated uniformly with fine nanoparticles. The TEM image of an individual composite nanofiber of this sample clearly reveals the core–shell structure with cellulose-derived carbon nanofiber as the core and tin oxide and molybdenum oxide nanoparticles anchored as the shell layer on the surface, and the thickness of the shell layer is about 61 nm (Fig. 2c). Since the relative atomic weight of Sn and Mo is close, it is difficult to distinguish the SnO₂ layer and MoO₂ layer only through TEM measurements. A high-resolution (HR)-TEM micrograph of the carbon–10%/SnO₂–20%/MoO₂ composite nanofiber surface displayed in Fig. 2d reveals the diameters of the SnO₂ and MoO₂ nanoparticles are about 5 and 6 nm, respectively; and the lattice spacing of 0.343 and 0.335 nm are consistent with the (–111) plane of the monoclinic MoO₂ [37], and the (110) plane of the rutile SnO₂ phase [2], respectively. The corresponding selected area electron diffraction (SAED) pattern contains a series of concentric circles (Fig. 2e), which reveals the polycrystalline features of the metal oxides in this composite, and the diffraction rings from the inside out are assigned to the MoO₂ (–111), MoO₂ (200), MoO₂ (–312), and SnO₂ (112), respectively. The elemental distribution of the carbon–10%/SnO₂–20%/MoO₂ composite nanofiber was further evaluated by EDX measurement, showing the signals of molybdenum, tin, and oxygen elements, which are distributed homogeneously along the carbon nanofiber core (Fig. 2f). In addition, the Mo signals distributed over the external edges of the nanofiber is stronger than that of Sn, indicating the SnO₂ layer is sandwiched between the core carbon nanofiber and the outer MoO₂ coating layer.

As for the carbon–13%/SnO₂–4%/MoO₂ and carbon–13%/SnO₂–12%/MoO₂ nanocomposites, similar hierarchically nanofibrous structures were observed, and the corresponding thickness of the coating layer on the carbon nanofiber surface was measured to be *ca.* 22 and 39 nm (Figs. S3 and 4), respectively. The control sample carbon–23%/MoO₂ also contains interconnected porous carbon nanofibers with MoO₂ nanoparticles randomly dispersed on the surfaces (Figs. S5a,

Fig. 2 Electron micrographs of the hierarchical nanofibrous carbon – 10%/SnO₂ – 20%/MoO₂ composite derived from commercial filter paper, where the deposition cycles of (PDDA/POM) bilayers by the LbL self-assembly process were repeated 15 times to fabricate the sample. **a** FE-SEM overview image of one microfiber composed by the sample. The inset is a photograph of the bulky material; **b** FE-SEM close view micrograph of the sample, displaying the nanofiber assemblies; **c** TEM image of an individual composite nanofiber of the sample; **d** HR-TEM micrograph and the corresponding **e** selected area electron diffraction (SAED) pattern of the composite nanofiber surface, confirming the presence of monoclinic MoO₂ and rutile SnO₂ phases; **f** energy dispersive X-ray (EDX) elemental maps of an individual composite nanofiber of the sample, showing the distribution of molybdenum, tin, carbon, and oxygen elements contained therein



b). As compared with the carbon@SnO₂@MoO₂ composites fabricated by the LbL self-assembled method, the MoO₂ nanoparticles obtained by the impregnation method appeared to be aggregated to some extent, therefore, the particle size is enlarged to be ca. 18 nm (Fig. S5c). As being utilized as anodic material for LIBs, the hierarchical network structures, small MoO₂ crystallite sizes, as well as the synergistic effect between MoO₂, SnO₂, and the porous carbon nanofiber held by the current carbon@SnO₂@MoO₂ composites, are expected to facilitate the Li ions and electrons transfer as well as alleviate the serious volume variation and agglomeration of the active particles upon the repeated discharge/charge processes, thus resulting in the enhanced lithium storage performances.

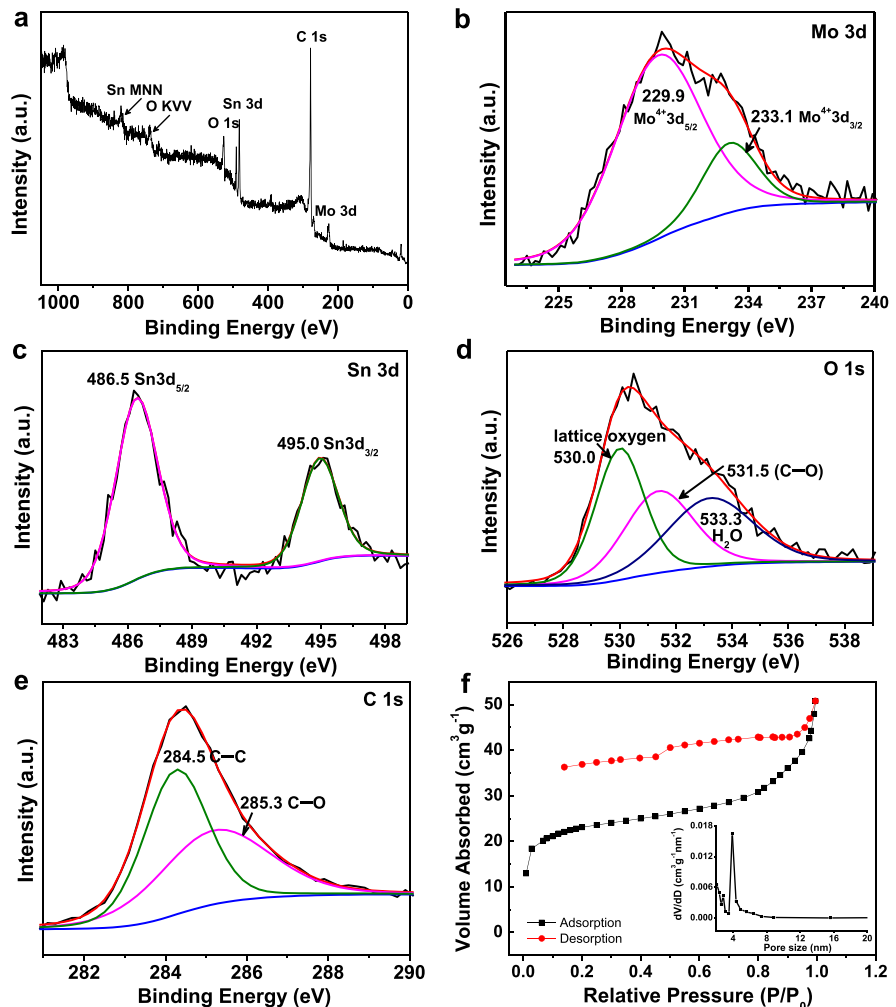
X-ray photoelectron spectroscopy (XPS) was applied to determine the oxidation state of molybdenum and tin elements contained in the carbon – 10%/SnO₂ – 20%/MoO₂ nanocomposite, and the whole spectrum of which validates the presence of molybdenum, tin, oxygen, and carbon elements (Fig. 3a). The high-resolution Mo 3d XPS spectrum of the sample (Fig. 3b) shows a doublet peak centered at 229.9 and 233.1 eV, with a typical spin energy separation of 3.2 eV, which are assigned to the Mo 3d_{5/2} and Mo 3d_{3/2} signals of molybdenum in the tetravalent state [48]. In addition, no signal from Mo⁶⁺ is observed in this spectrum, confirming the initial POM cluster was completely transformed into MoO₂ by the heating treatment. For the Sn 3d region (Fig. 3c), the peaks

of Sn $3d_{5/2}$ and Sn $3d_{3/2}$ are located at 486.5 and 495.0 eV, respectively, and the 8.5 eV peak separation of which indicates the existence of Sn⁴⁺ in the nanocomposite [54]. Figure 3d presents the HR-XPS spectrum of the O1s region, and it is deconvoluted into three peaks: the one at 530.1 eV is corresponding to the lattice oxygen of Mo–O and Sn–O bonds formed in MoO₂ and SnO₂ [61, 62]; the other at 531.5 eV is ascribed to the O²⁻ species bonded with C atoms in the porous carbon nanofiber derived from natural cellulose substance [27], and the third one located at 533.3 eV is related to the chemisorbed water [63], respectively. The deconvoluted C 1s spectrum (Fig. 3e) reveals two carbon components, the peak at 284.5 eV is indexed to the C–C bond arising from the aromatization reaction of cellulose during carbonization treatment [64], and the peak at

285.2 eV is related to C–O group stemming from small residual oxygenated functional groups upon carbonization of cellulose [58]. These results demonstrate the formation of the carbon@SnO₂@MoO₂ hybrid, which are in good accordance with the XRD, Raman, and HR-TEM results discussed above.

Figure 3f represents the nitrogen adsorption–desorption isotherm and the pore-size distribution of the nanofibrous carbon–10%/SnO₂–20%/MoO₂ composite. It is seen that the isotherm is classified as type IV with an H2-type hysteresis loop based on the IUPAC classification, demonstrating the existence of mesoporous and three-dimensional network structure in this composite [64]. Moreover, the desorption branch of the isotherm was not closed in the low-pressure regions, which is caused by the irregular nanopores contained in the carbon nanofibers of

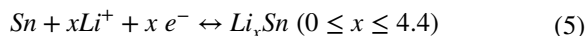
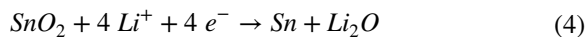
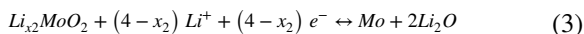
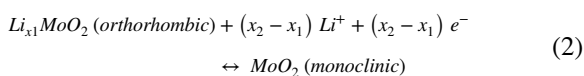
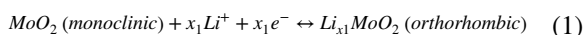
Fig. 3 XPS general spectrum (a); high-resolution XPS spectra of Mo(3 d) (b), Sn (3 d) (c), O (1 s) (d), C (1 s) (e) regions, and nitrogen adsorption–desorption isotherm as well as the pore size distribution profile (f) of the nanofibrous carbon–10%/SnO₂–20%/MoO₂ composite



this composite [65, 66]. The pore size distribution is mainly centered at 3.88 nm, and the total pore volume as well as the BET-specific surface area are measured to be $0.03 \text{ cm}^3 \text{ g}^{-1}$ and $74.5 \text{ cm}^2 \text{ g}^{-1}$, respectively. These results reveal that the mesopores existed in the carbon–10%/SnO₂–20%/MoO₂ composite, which would promote the electrode/electrolyte contact and shorten the diffusion length for Li-ions, thus resulting in an improved lithium storage behavior.

Electrochemical properties

As described above, the bio-inspired hierarchically three-dimensional network structures, small size of the metal oxide nanoparticles, and the effective synergistic interaction of the carbon nanofiber, SnO₂, and MoO₂ components possessed by the present nanofibrous carbon@SnO₂@MoO₂ composites would be beneficial for the enhanced electrochemical performances as being employed as anodic materials for LIBs. Figure 4a displays the cyclic voltammetry (CV) curves of the carbon–10%/SnO₂–20%/MoO₂ composite anode for the initial four cycles at a scan rate of 0.2 mV s^{-1} in the potential range of 0.01–3.0 V vs. Li/Li⁺. In the first cathodic sweep process of the sample, the two reduction peaks that appeared at 1.21 and 1.53 V are attributed to the phase transition of partially lithiated Li_xMoO₂ from monoclinic to orthorhombic phase and from orthorhombic to monoclinic phase, respectively [34, 67]. And the peak at 0.74 V is caused by the insertion of Li ions into SnO₂ to yield metallic Sn and amorphous Li₂O [68], as well as the formation of solid electrolyte interface (SEI) films [50]. The strong cathodic peak at about 0.02 V is corresponding to the conversion reaction from Li_xMoO₂ to metallic Mo and Li₂O [69], as well as lithiation of Sn to form the Li_xSn alloy [68]. The related electrochemical reactions are given as follows [31, 70]:



In the first anodic sweep process, the reversible oxidation peak at 0.53 V is assigned to the delithiation process of the Li_xSn alloy [53, 54], and the anodic peaks at 1.28 and 1.70 V are related to the generation of tin oxide due to the partial recombination reaction between metallic Sn and Li₂O [53], as well as the reversible phase transition process (monoclinic–orthorhombic–monoclinic) for the removal of Li-ions to give MoO₂ [31]. From the second cycle onward, the three pairs of the redox peaks at 0.02/0.53, 1.12/1.31, and 1.58/1.70 V are observed; the first one involves the highly reversible alloying/de-alloying process of metallic Sn [54] and the conversion reaction of Li_xMoO₂ to metallic Mo [69]. The other two correspond to the reversible conversion of Li_xMoO₂ and MoO₂ caused by the lithiation/delithiation process [34, 67], respectively. Moreover, other redox peaks that appeared at 0.91/1.21 V are caused by the lithiation/delithiation of carbon species derived from cellulose substance [54]. The overlapped CV profiles after the first cycle indicate the good electrochemical reversibility and cyclability of the nanocomposite in the following lithium insertion/extraction processes. For the cellulose, substance derived carbon–13%/SnO₂–12%/MoO₂, carbon–13%/SnO₂–4%/MoO₂, and carbon–23%/MoO₂ composites, similar CV features were observed (Fig. S6), except that the redox peaks intensity of 0.02/0.53 V became weaker owing to the decreased SnO₂ contents.

Figure 4b displays the galvanostatic discharge/charge (GDC) voltage profiles of the nanofibrous carbon–10%/SnO₂–20%/MoO₂ composite electrode in the 1st, 2nd, 10th, 20th, and 50th cycles at a constant current rate of 100 mA g^{-1} between 0.01 and 3.0 V vs. Li/Li⁺. During the first lithiation process, a small potential plateau at ca. 1.24 V is caused by the phase transition related to the generation of the Li_xMoO₂ phase (Eqs. 1,2) [34, 67]. The slope that appeared at 1.0–0.5 V is assigned to the lithiation process of SnO₂ yielding metallic Sn and Li₂O phase (Eq. 4) [68], as well as the formation of the Li_xC phase [54] and SEI films [50]. The long plateau below 0.40 V is caused by the conversion reaction of Li_xMoO₂ to

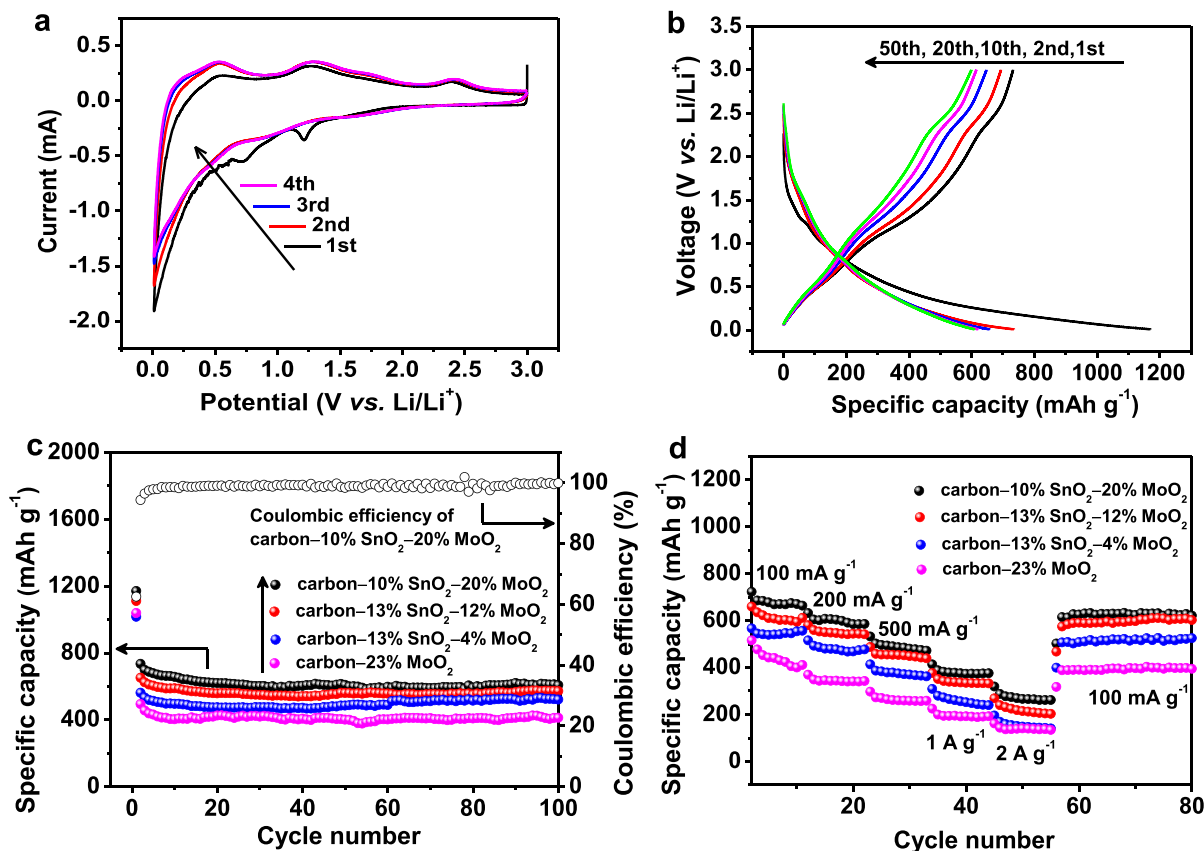


Fig. 4 Electrochemical performances of the carbon@SnO₂@MoO₂ nanocomposite utilized as anodic material for LIBs, the sample was synthesized with 15 cycles of (PDDA/POM) bilayers deposited onto SnO₂-gel pre-coated cellulose nanofiber surface (sample carbon-10%/SnO₂-20%/MoO₂) unless otherwise stated. **a** Cyclic voltammograms of the sample scanned at 0.2 mV s⁻¹ within the potential window of 0.01–3.0 V vs. Li/Li⁺; **b** galvanostatic charge/discharge profiles of the sample at the 1st, 2nd, 10th, 20th, and 50th cycles meas-

ured at a constant current rate of 100 mA g⁻¹ between 0.01 and 3.0 V; **c** galvanostatic discharge cycling performances of the carbon@SnO₂@MoO₂ nanocomposites with varied MoO₂ contents and carbon-23%/MoO₂ hybrid cycled at a current rate of 100 mA g⁻¹, as well as Coulombic efficiency of the carbon-10%/SnO₂-20%/MoO₂ composite; **d** rate capabilities of the corresponding materials from the second cycle at different current densities

produce metallic Mo and Li₂O matrix (Eq. 3) as well as the alloying process of Sn (Eq. 5) [68, 69]. All the potential plateaus agree well with the CV results described above. The initial discharge and charge capacities of this composite are 1170.3 and 732.1 mAh g⁻¹, respectively, with a Coulombic efficiency of 62.6%. The low Coulombic efficiency obtained in the first cycle is common for the metal oxide-based electrodes, which is mainly attributed to the irreversible electrochemical processes such as decomposition of organic electrolyte to form excessive SEI films coated on the surfaces of the active species and partial Li-ions trapped inside the crystalline lattices

of the metal oxide, as well as the irreversible reduction of SnO₂ [71, 72]. The Coulombic efficiency was increased to 94.4% in the second cycle and continually increased to be 97.9% after five cycles. In addition, the GDC profiles were similar to those obtained from the second cycle, indicating a good cycling stability of this composite anode; and the discharge capacity of the sample decreased to be 609.3 mAh g⁻¹ after 50 cycles, and the capacity retention is 82.9% according to the 50th/2nd discharge values. As for the carbon-13%/SnO₂-4%/MoO₂ and carbon-13%/SnO₂-12%/MoO₂ nanocomposites (Fig. S7a, b), the GDC voltage curves are similar to that of the

carbon–10%/SnO₂–20%/MoO₂ composite, and the initial discharge/charge capacities are 1111.3/652.1 and 1016.6/565.5 mAh g⁻¹, respectively. Furthermore, the discharge capacities of these two samples slowly decreased in the following cycles and reached 560.8 and 485.2 mAh g⁻¹ at the 50th cycle. For the control carbon–23%/MoO₂ composite (Fig. S7c), both the discharge and charge voltage plateaus are compliant with the lithiation/delithiation features of MoO₂ and carbon species derived from the carbonization of cellulose. The first cycle discharge capacity is 1038.9 mAh g⁻¹ with the corresponding Coulombic efficiency of 45.8 %, and the specific capacity faded quickly in the initial ten cycles and gradually down to 401.5 mAh g⁻¹ after 50 discharge/charge cycles.

Figure 4c depicts the galvanostatic discharge cycling performances of the cellulose substance derived carbon@SnO₂@MoO₂ and carbon–23%/MoO₂ composites measured at a current density of 100 mA g⁻¹ over the potential window of 0.01–3.0 V. For the nanofibrous carbon–10%/SnO₂–20%/MoO₂ anode, the specific capacity of it decayed quickly in the first ten cycles from 1170.3 to 656.9 mAh g⁻¹, and then maintained a relatively stable state with a Coulombic efficiency higher than 98.5%. After 100 discharge/charge processes, the reversible capacity of the composite was restored to 608.1 mAh g⁻¹; this value is readily acceptant for this carbon–10%/SnO₂–20%/MoO₂ composite with relatively low contents of SnO₂ (10%) and MoO₂ (20%). The capacity delivered by the present composite is calculated as follows:

$$C(C@SnO_2@MoO_2)_{theo} = C(C)_{theo} * mass\%(C) + C(SnO_2)_{theo} * mass\%(SnO_2) + C(MoO_2)_{theo} * mass\%(MoO_2) \quad (6)$$

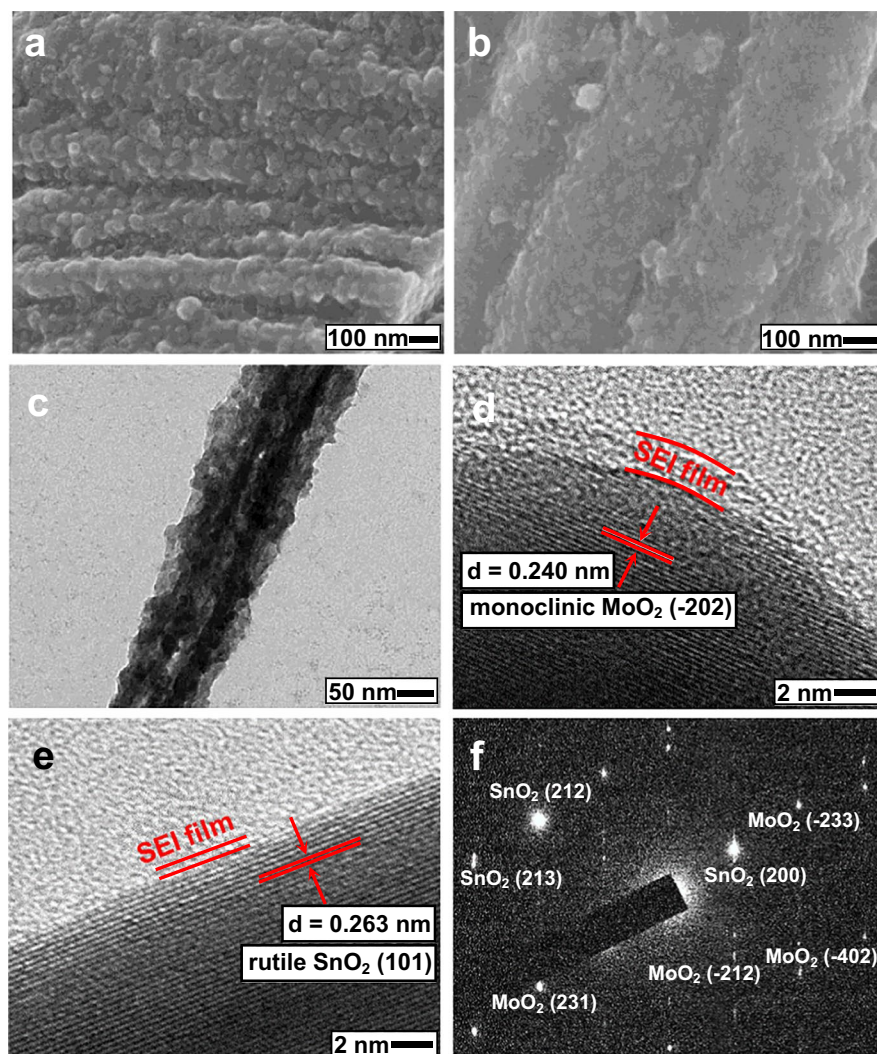
Since the theoretical reversible capacities of carbon, MoO₂, and SnO₂ are 372, 838, and 782 mAh g⁻¹, respectively [34, 53], and the corresponding mass fraction of each component is 70, 20, and 10 wt.%, respectively, the theoretical reversible capacity of this composite was calculated to be 506.2 mAh g⁻¹, which is lower than the experimental value of 608.1 mAh g⁻¹. This is ascribed to the hierarchical three-dimensional network structures as well as the synergistic effect between carbon, SnO₂, and MoO₂ components possessed by the composite. The unique multi-level nanostructure of the composite facilitates high Li-ion flux across the interface, shortens the transmission path for both Li ions and

electrons, and provides abundant active sites for lithium accommodation. The main active components of SnO₂ and MoO₂ predominately contribute to the high lithium storage capacity, and the filter paper-derived carbon nanofibers not only improve the electro-conductivity of the composite but also act as buffer matrix, relaxing the serious volume variation and preventing the agglomeration of the SnO₂ and MoO₂ nanoparticles upon repeated lithiation/delithiation processes. Besides, the metallic Mo and Sn formed in the discharge process serve as the physical adsorption sites for Li ions and participate in the lithiation reaction, thus contributing to the additional capacity [73]. Moreover, the Li₂O phase formed also works as a buffer matrix for Mo and Sn to relax the volume change to some extent, thus giving a high practical capacity.

As compared with some preceding reports on MoO₂/C and SnO₂/C anodic materials, the current nanofibrous carbon–10%/SnO₂–20%/MoO₂ composite possesses a superior lithium storage performance. For instance, the carbon-coated MoO₂ nanofibers prepared by an electrospinning method combined with controlled air-stabilization and reduction-carbonization released a specific capacity of 582.7 mAh g⁻¹ after 50 discharge/charge cycles at a current rate of 100 mA g⁻¹ [74], and the MoO₂/C hybrid with ultrafine MoO₂ nanoparticles homogeneously distributed in a carbon matrix fabricated by the impregnation-reduction-carbonization route gave a capacity of ca. 550 mAh g⁻¹ after 50 cycles at the same current rate [75]. Furthermore, the discharge capacity of the carbon–10%/SnO₂–20%/MoO₂ composite was 475.3 mAh g⁻¹ cycled at a higher current density of 500 mA g⁻¹ (as displayed below), which was higher than that of the cotton/rGO/carbon-coated SnO₂ nanoparticle-composites prepared by an impregnation-hydrothermal route combined with carbonization treatment (361.1 mAh g⁻¹ at 400 mA g⁻¹) [76]. It is obvious that the current nanofibrous carbon–10%/SnO₂–20%/MoO₂ composite displays excellent lithium storage behavior.

As for the carbon–13%/SnO₂–4%/MoO₂ and carbon–13%/SnO₂–12%/MoO₂ nanocomposites, similar stable discharge cycling capabilities were obtained, and the discharge capacities after 100 cycles remained at 572.2 and 521.8 mAh g⁻¹, respectively, which are lower than those of the carbon–10%/SnO₂–20%/MoO₂ hybrid due to the lower MoO₂ contents contained therein, revealing that higher MoO₂ content in the composite would contribute to the better electrochemical performance.

Fig. 5 Electron micrographs of the carbon–10%/SnO₂–20%/MoO₂ composite utilized as anodic material for LIBs after 100 discharge/charge cycles. **a,b** FE-SEM images of the sample, revealing the structural integrity of the composite; **c** TEM micrograph of an individual composite nanofiber isolated from the sample; **d,e** HR-TEM images and relevant **f** SAED pattern of the composite nanofiber surface, demonstrating the crystalline nature of molybdenum dioxide and tin oxide species have partially remained



For the control sample carbon–23%/MoO₂, dramatic capacity decaying occurred in the initial ten cycles, where the corresponding discharge capacity declined to 411.8 mAh g⁻¹ at the 100th cycle, which is still higher than the theoretical capacity of the graphite-based anode. Compared with the carbon–23%/MoO₂, the enhanced cycling stability of the carbon@SnO₂@MoO₂ hybrid benefits from its unique hierarchically multi-level nanostructure, which offers a high surface area for facilitating the electrode–electrolyte contact. Moreover, the nanofibrous carbon core uniformly coated with SnO₂ and MoO₂ layer works as a buffer matrix to effectively accommodate the drastic volume change and restrain the agglomeration of the active components during

the cycling, thus maintaining the structural integrity of the anodic material upon cycling and resulting in improved cycling performance.

Figure 4d shows the rate capabilities of the nanofibrous carbon@SnO₂@MoO₂ and carbon–23%/MoO₂ composites under various current densities. It is seen that the carbon–10%/SnO₂–20%/MoO₂ composite presented the best rate performance, and the discharge capacities of which were retained at 670.7, 585.8, 475.3, 375.6, and 261.5 mAh g⁻¹ at the current rates of 100, 200, 500, 1000, and 2000 mA g⁻¹, respectively. Once the current was switched back to 100 mA g⁻¹, the specific capacity recovered to 614.7 mAh g⁻¹, and kept stable in the following cycles. The capacity retention is 85.1% based on the 2nd capacity value. The good

capacity recovery capability is profited from the unique hierarchical nanostructure of the composite as well as the effective synergistic effect between each component contained therein. As for the carbon–13%/SnO₂–4%/MoO₂ and carbon–13%/SnO₂–12%/MoO₂ composites, the corresponding capacities were lower than that of the carbon–10%/SnO₂–20%/MoO₂ sample, revealing the higher MoO₂ content in the carbon@SnO₂@MoO₂ composites contribute to the good rate performance and improved specific capacity. While for the control sample carbon–23%/MoO₂, the specific capacity faded sharply in the first ten cycles, and declined to 134.3 mAh g⁻¹ when the current rate increased to 2000 mA g⁻¹. In addition, it is noteworthy that although the capacities of all the samples gradually declined along with the increment of the current density, the cycling stabilities even under high currents were still satisfactory due to the presence of the carbon nanofibers to maintain the structural integrity of composite electrode upon the repeated discharge/charge cycling processes. And the structural integrity of the nanofibrous carbon–10%/SnO₂–20%/MoO₂ composite after 100 cycling processes was further examined by the electron microscope measurements. The FE-SEM micrograph of this nanocomposite reveals the original hierarchically nanofibrous structure was still maintained and no obvious crack/fracture was observed (Fig. 5a). TEM image of the sample also confirms the integrity of the initial core–shell structure in the composite. Moreover, it is clearly seen that the excessive SEI films are coated on the active species surface due to the long-term discharge/charge cycles (Fig. 5b). The polycrystalline nature of the MoO₂ and SnO₂ were partially retained, as demonstrated by HR-TEM examinations (Figs. 5c–e). The good structural stability of the sample is attributed to the cellulose substance derived carbon nanofibers, which effectively relax the drastic volume change of the MoO₂ and SnO₂ nanoparticles upon the repeated lithiation/delithiation processes, resulting in the good capacity maintainability of the carbon–10%/SnO₂–20%/MoO₂ anode.

Conclusion

In summary, a new hierarchically nanofibrous carbon@SnO₂@MoO₂ composite was synthesized by the LbL self-assembly of POM/PDDA double layers on the SnO₂-gel precoated cellulose nanofibers of bulk cellulose substance (ordinary filter paper),

followed by carbonization treatment. The resultant composite duplicated the sophisticated three-dimensional network morphologies and the macro-to-nano structural characters of the original cellulose substance. It was composed of SnO₂ thin layer coated carbon nanofibers with MoO₂ nanoparticles immobilized as the outer coating layer on the outmost surfaces. When utilized as an anodic material for LIBs, the composite exhibited enhanced lithium storage properties in terms of high specific capacity, excellent cycling stability, and good rate performance. This is attributed to the attractive structural advantages of the composite and the effective synergistic interaction between MoO₂, SnO₂, and carbon nanofiber contained therein, which promote the electrolyte/active species contact, facilitate the Li-ions and electrons transfer, as well as buffer the severe volume change of MoO₂ and SnO₂ components upon the repeated lithiation/delithiation processes. Biomimetic synthesis combined with the LbL self-assemble technique shed new light on the design and development of novel nanoarchitectonics for energy-related purposes, especially for high-performance electrode materials with fascinating structures inherited from the natural substances and the specific functionalities of the guest species.

Funding This work was supported by the Zhejiang Provincial Natural Science Foundation of China (LY16B010001).

Declarations

Conflict of interest The authors declare that they have no conflict of interest.

References

1. Gwon H, Hong J, Kim H, Seo DH, Jeon S, Kang K (2014) Recent progress on flexible lithium rechargeable batteries. *Energy Environ Sci* 7:538–551. <https://doi.org/10.1039/C3EE42927J>
2. Tang Y, Wu D, Chen S, Fan Z, Jia J, Feng X (2013) Highly reversible and ultra-fast lithium storage in mesoporous graphene-based TiO₂/SnO₂ hybrid nanosheets. *Energy Environ Sci* 6:2447–2451. <https://doi.org/10.1039/C3EE40759D>
3. Ji L, Lin Z, Alcoutlabi M, Zhang X (2011) Recent developments in nanostructured anode materials for rechargeable lithium-ion batteries. *Energy Environ Sci* 4:2682–2699. <https://doi.org/10.1039/C0EE00699H>

4. Jiang J, Li Y, Liu J, Huang X (2011) Building one-dimensional oxide nanostructure arrays on conductive metal substrates for lithium-ion battery anodes. *Nanoscale* 3:45–58. <https://doi.org/10.1039/C0NR00472C>
5. Zhang J, Yu A (2015) Nanostructured transition metal oxides as advanced anodes for lithium-ion batteries. *Sci Bull* 60:823–838. <https://doi.org/10.1007/s11434-015-0771-6>
6. Ariga K (2020) Nano-architectonics for coordination assemblies at interfacial media. *Adv Inorg Chem* 76:239–268. <https://doi.org/10.1016/bs.adioch.2020.03.005>
7. Ariga K (2020) The evolution of molecular machines through interfacial nanoarchitectonics: from toys to tools. *Chem Sci* 11:10594–10604. <https://doi.org/10.1039/D0SC03164J>
8. Ariga K (2020) Nanoarchitectonics: bottom-up creation of functional materials and systems. *Beilstein J Nanotechnol* 11:450–452. <https://doi.org/10.3762/bjnano.11.36>
9. Ariga K (2021) Progress in molecular nanoarchitectonics and materials nanoarchitectonics. *Molecules* 26:1621. <https://doi.org/10.3390/molecules26061621>
10. Ariga K, Shionoya M (2021) Nanoarchitectonics for coordination asymmetry and related chemistry. *Bull Chem Soc Jpn* 94:839–859. <https://doi.org/10.1246/bcsj.20200362>
11. Abe H, Liu J, Ariga K (2016) Catalytic nanoarchitectonics forenvironmentally compatible energy generation. *Mater Today* 19:12–18. <https://doi.org/10.1016/j.mattod.2015.08.021>
12. Khan AH, Ghosh S, Pradhan B, Dalui A, Shrestha LK, Acharya S, Ariga K (2017) Two-dimensional (2D) nanomaterials towards electrochemical nanoarchitectonics in energy-related applications. *Bull Chem Soc Jpn* 90:627–648. <https://doi.org/10.1246/bcsj.20170043>
13. Rydzek G, Ji Q, Li M, Schaaf P, Hill JP, Boulmedais F, Ariga K (2015) Electrochemical nanoarchitectonicsand layer-by-layer assembly: Frombasicsto future. *Nano Today* 10:138–167. <https://doi.org/10.1016/j.nantod.2015.02.008>
14. Shrestha RG, Shrestha LK, Ariga K (2021) Carbon nanoarchitectonics for energy and related applications. *C* 7:73 <https://doi.org/10.3390/c7040073>
15. Wu HB, Chen JS, Hng HH, Lou XW (2012) Nanostructured metal oxide-based materials as advanced anodes for lithium-ion batteries. *Nanoscale* 4:2526–2542. <https://doi.org/10.1039/C2NR11966H>
16. Idota Y, Kubota T, Matsufuji A, Maekawa Y, Miyasaka T (1997) Tin-based amorphous oxide: a high-capacity lithium-ion-storage material. *Science* 276:1395–1397. <https://doi.org/10.1126/science.276.5317.1395>
17. Liu H, Long D, Liu X, Qiao W, Zhan L, Ling L (2009) Facile synthesis and superior anodic performance of ultrafine SnO₂-containing nanocomposites. *Electrochim Acta* 54:5782–5788. <https://doi.org/10.1016/j.electacta.2009.05.030>
18. Liu L, Xie F, Lyu J, Zhao T, Li T, Choi BG (2016) Tin-based anode materials with well-designed architectures for next generation lithium-ion batteries. *J Power Sources* 321:11–35. <https://doi.org/10.1016/j.jpowsour.2016.04.105>
19. Zhu J, Lu Z, Oo MO, Hng HH, Ma J, Zhang H, Yan Q (2011) Synergetic approach to achieve enhanced lithium ion storage performance in ternary phased SnO₂-Fe₂O₃/RGO composite nanostructures. *J Mater Chem* 21:12770–12776. <https://doi.org/10.1039/C1JM12447A>
20. Petnikota S, Teo KW, Chen L, Sim A, Marka SK, Reddy MV, Srikanth VVSS, Adams S, Chowdari BVR (2016) Exfoliated graphene oxide/MoO₂ composites as anode materials in lithium-ion batteries: an insight into intercalation of Li and conversion mechanism of MoO₂. *ACS Appl Mater Interfaces* 8:10884–10896. <https://doi.org/10.1021/acsami.6b02049>
21. Tan X, Cui C, Wu S, Qiu B, Wang L, Zhang J (2017) Nitrogen-doped mesoporous carbon-encapsulated MoO₂ nanobelts as a high-capacity and stable host for lithium-ion storage. *Chem Asian J* 12:36–40. <https://doi.org/10.1002/asia.201601521>
22. Park J, Choi I, Lee MJ, Kim MH, Lim T, Park KH, Jang J, Oh SM, Cho SK, Kim JJ (2014) Effect of fluoroethylene carbonate on electrochemical battery performance and the surface chemistry of amorphous MoO₂ lithium-ion secondary battery negative electrodes. *Electrochim Acta* 132:338–346. <https://doi.org/10.1016/j.electacta.2014.03.173>
23. Guo B, Fang X, Li B, Shi Y, Ouyang C, Hu YS, Wang Z, Stucky GD, Chen L (2012) Synthesis and lithium storage mechanism of ultrafine MoO₂ nanorods. *Chem Mater* 24:457–463. <https://doi.org/10.1021/cm202459r>
24. Yang LC, Gao QS, Zhang YH, Tang Y, Wu YP (2008) Tremella-like molybdenum dioxide consisting of nanosheets as an anode material for lithium ion battery. *Electrochem Commun* 10:118–122. <https://doi.org/10.1016/j.elecom.2007.11.009>
25. Zhao X, Cao M, Liu B, Tian Y, Hu C (2012) Interconnected core-shell MoO₂ microcapsules with nanorod-assembled shells as high-performance lithium-ion battery anodes. *J Mater Chem* 22:13334–13340. <https://doi.org/10.1039/C2JM30862B>
26. Zeng L, Zheng C, Deng C, Ding X, Wei M (2013) MoO₂-ordered mesoporous carbon nanocomposite as an anode material for lithium-ion batteries. *ACS Appl Mater Interfaces* 5:2182–2187. <https://doi.org/10.1021/am303286n>
27. Gao Q, Zhao X, Xiao Y, Zhao D, Cao M (2014) A mild route to mesoporous MO₂C-C hybrid nanospheres for high performance lithium-ion batteries. *Nanoscale* 6:6151–6157. <https://doi.org/10.1039/C3NR06678A>
28. Xia F, Hu X, Sun Y, Luo W, Huang Y (2012) Layer-by-layer assembled MoO₂-graphene thin film as a high-capacity and binder-free anode for lithium-ion batteries. *Nanoscale* 4:4707–4711. <https://doi.org/10.1039/C2NR30742A>
29. Huang ZX, Wang Y, Zhu YG, Shi Y, Wong JI, Yang HY (2014) 3D graphene supported MoO₂ for high performance binder-free lithium ion battery. *Nanoscale* 6:9839–9845. <https://doi.org/10.1039/C4NR01744G>
30. Palanisamy K, Kim Y, Kim H, Kim JM, Yoon WS (2015) Self-assembled porous MoO₂/graphene microspheres towards high performance anodes for lithium ion batteries. *J Power Sources* 275:351–361. <https://doi.org/10.1016/j.jpowsour.2014.11.001>
31. Qiu S, Lu G, Liu J, Lyu H, Hu C, Li B, Yan X, Guo J, Guo Z (2015) Enhanced electrochemical performances of MoO₂ nanoparticles composited with carbon nanotubes for lithium-ion battery anodes. *RSC Adv* 5:87286–87294. <https://doi.org/10.1039/C5RA17147D>

32. Zhou E, Wang C, Shao M, Deng X, Xu X (2017) MoO₂ Nanoparticles grown on carbon fibers as anode materials for lithium-ion batteries. *Ceram Int* 43:760–765. <https://doi.org/10.1016/j.ceramint.2016.10.006>
33. Zeng L, Huang X, Chen X, Zheng C, Liu R, Chen G, Qian Q, Chen Q, Wei M (2016) Ethanol thermal reduction synthesis of hierarchical MoO₂-C hollow spheres with high rate performance for lithium ion batteries. *RSC Adv* 6:105558–105564. <https://doi.org/10.1039/C6RA22792A>
34. Zhang HJ, Wu TH, Wang KX, Wu XY, Chen XT, Jiang YM, Wei X, Chen JS (2013) Uniform hierarchical MoO₂/carbon spheres with high cycling performance for lithium ion batteries. *J Mater Chem A* 1:12038–12043. <https://doi.org/10.1039/C3TA12566A>
35. Xia G, Liu D, Zheng F, Yang Y, Su J, Chen Q (2016) Preparation of porous MoO₂@C nano-octahedrons from a polyoxometalate-based metal-organic framework for highly reversible lithium storage. *J Mater Chem A* 4:12434–12441. <https://doi.org/10.1039/C6TA03491H>
36. Bhaskar A, Deepa M, Rao TN (2013) MoO₂/multiwalled carbon nanotubes (MWCNT) hybrid for use as a li-ion battery anode. *ACS Appl Mater Interfaces* 5:2555–2566. <https://doi.org/10.1021/am3031536>
37. Chen A, Li C, Tang R, Yin L, Qi Y (2013) MoO₂-ordered mesoporous carbon hybrids as anode materials with highly improved rate capability and reversible capacity for lithium-ion battery. *Phys Chem Chem Phys* 15:13601–13610. <https://doi.org/10.1039/C3CP51255J>
38. Liu B, Zhao X, Tian Y, Zhao D, Hu C, Cao M (2013) A simple reduction process to synthesize MoO₂/C composites with cage-like structure for high-performance lithium-ion batteries. *Phys Chem Chem Phys* 15:8831–8837. <https://doi.org/10.1039/C3CP44707C>
39. Ariga K, Ji Q, Hill JP, Vinu A (2009) Coupling of soft technology (layer-by-layer assembly) with hard materials (mesoporous solids) to give hierarchic functional structures. *Soft Matter* 5:3562–3571. <https://doi.org/10.1039/B909397D>
40. He Q, Cui Y, Ai S, Tian Y, Li J (2009) Self-assembly of composite nanotubes and their applications. *Curr Opin Colloid Interface Sci* 14:115–125. <https://doi.org/10.1016/j.cocis.2008.09.005>
41. He Q, Cui Y, Li J (2009) Molecular assembly and application of biomimetic microcapsules. *Chem Soc Rev* 38:2292–2303. <https://doi.org/10.1039/B816475B>
42. Jia Y, Li J (2015) Molecular assembly of Schiff base interactions: construction and application. *Chem Rev* 115:1597–1621. <https://doi.org/10.1021/cr400559g>
43. Li J, Möhwalld H, An Z, Lu G (2005) Molecular assembly of biomimetic microcapsules. *Soft Matt* 1:259–264. <https://doi.org/10.1039/B506092N>
44. Yan X, Zhu P, Li J (2010) Self-assembly and application of diphenylalanine-based nanostructures. *Chem Soc Rev* 39:1877–1890. <https://doi.org/10.1039/B915765B>
45. Malgras V, Ji Q, Kamachi Y, Mori T, Shieh FK, Wu KCW, Ariga K, Yamauchi Y (2015) Templated synthesis for nanoarchitected porous materials. *Bull Chem Soc Jpn* 88:1171–1200. <https://doi.org/10.1246/bcsj.20150143>
46. Ding Y, Bai W, Sun J, Wu Y, Memon MA, Wang C, Liu C, Huang Y, Geng J (2016) Cellulose tailored anatase TiO₂ nanospindles in three-dimensional graphene composites for high-performance supercapacitors. *ACS Appl Mater Interfaces* 8:12165–12175. <https://doi.org/10.1021/acsami.6b02164>
47. Jia D, Chen Y, Huang J (2017) A bio-inspired nanofibrous titania/silicon composite as an anode material for lithium-ion batteries. *ChemNanoMat* 3:120–129. <https://doi.org/10.1002/cnma.201600332>
48. Li BB, Liang YQ, Yang XJ, Cui ZD, Qiao SZ, Zhu SL, Li ZY, Yin K (2015) MoO₂-CoO coupled with a macroporous carbon hybrid electrocatalyst for highly efficient oxygen evolution. *Nanoscale* 7:16704–16714. <https://doi.org/10.1039/C5NR04666A>
49. Li S, Wang M, Luo Y, Huang J (2016) Bio-inspired hierarchical nanofibrous Fe₃O₄-TiO₂-carbon composite as a high-performance anode material for lithium-ion batteries. *ACS Appl Mater Interfaces* 8:17343–17351. <https://doi.org/10.1021/acsami.6b05206>
50. Li J, Huang J (2015) A nanofibrous polypyrrole/silicon composite derived from cellulose substance as the anode material for lithium-ion batteries. *Chem Commun* 51:14590–14593. <https://doi.org/10.1039/C5CC05300E>
51. Li S, Huang J (2015) A nanofibrous silver-nanoparticle/titania/carbon composite as an anode material for lithium ion batteries. *J Mater Chem A* 3:4354–4360. <https://doi.org/10.1039/C4TA06562J>
52. Ouyang W, Sun J, Memon J, Wang C, Geng J, Huang Y (2013) Scalable preparation of three-dimensional porous structures of reduced graphene oxide/cellulose composites and their application in supercapacitors. *Carbon* 62:501–509. <https://doi.org/10.1016/j.carbon.2013.06.049>
53. Wang M, Li S, Zhang Y, Huang J (2015) Hierarchical SnO₂/carbon nanofibrous composite derived from cellulose substance as anode material for lithium-ion batteries. *Chem Eur J* 21:16195–16202. <https://doi.org/10.1002/chem.201502833>
54. Wang K, Wang M, Huang J (2016) Natural-cellulose-derived tin-nanoparticle/carbon-nanofiber composite as anodic material in lithium-ion batteries. *ChemNanoMat* 2:1040–1046. <https://doi.org/10.1002/cnma.201600225>
55. Zhao B, Yang G, Ran R, Kwak C, Jung DW, Park HJ, Shao Z (2014) Facile synthesis of porous MgO-CaO-SnO_x nanocubes implanted firmly on in situ formed carbon paper and their lithium storage properties. *J Mater Chem A* 2:9126–9133. <https://doi.org/10.1039/C4TA00805G>
56. Xu Z, Wang H, Li Z, Kohandehghan A, Ding J, Chen J, Cui K, Mitlin D (2014) Sulfur refines MoO₂ distribution enabling improved lithium ion battery performance. *J Phys Chem C* 118:18387–18396. <https://doi.org/10.1021/jp504721y>
57. Ashok J, Reddy PS, Raju G, Subrahmanyam M, Venugopal A (2009) Catalytic decomposition of methane to hydrogen and carbon nanofibers over Ni-Cu-SiO₂ catalysts. *Energy Fuel* 23:5–13. <https://doi.org/10.1021/ef8003976>
58. Wang K, Huang J (2019) Natural cellulose derived nanofibrous Ag-nanoparticle/SnO₂/carbon ternary composite as an anodic material for lithium-ion batteries. *J Phys Chem Solids* 126:155–163. <https://doi.org/10.1016/j.jpccs.2018.11.025>
59. Jiang S, Zhao B, Ran R, Cai R, Tadé MO, Shao Z (2014) A freestanding composite film electrode stacked from hierarchical electrospun SnO₂ nanorods and graphene

- sheets for reversible lithium storage. *RSC Adv* 4:9367–9371. <https://doi.org/10.1039/C3RA47840H>
60. Li S, Huang J (2016) Cellulose-rich nanofiber-based functional nanoarchitectures. *Adv Mater* 28:1143–1158. <https://doi.org/10.1002/adma.201501878>
61. Bai S, Chen S, Chen L, Zhang K, Luo R, Li D, Liu CC (2012) Ultrasonic synthesis of MoO₃ nanorods and their gas sensing properties. *Sens Actuators B* 174:51–58. <https://doi.org/10.1016/j.snb.2012.08.015>
62. Bai S, Liu J, Guo J, Luo R, Li D, Song Y, Liu CC, Chen A (2017) A facile preparation of SnO₂/NiO composites and enhancement of sensing performance to NO₂. *Sens Actuators B* 249:22–29. <https://doi.org/10.1016/j.snb.2017.03.121>
63. Li Y, Hu Y, Shen J, Jiang H, Min G, Qiu S, Song Z, Sun Z, Li C (2015) Rapid flame synthesis of internal Mo⁶⁺ doped TiO₂ nanocrystals in situ decorated with highly dispersed MoO₃ clusters for lithium ion storage. *Nanoscale* 7:18603–18611. <https://doi.org/10.1039/C5NR05586E>
64. Liu X, Gu Y, Huang J (2010) Hierarchical, titania-coated, Carbon nanofibrous material derived from a natural cellulosic substance. *Chem Eur J* 16:7730–7740. <https://doi.org/10.1002/chem.201000436>
65. Nowicki P, Pietrzak R, Wachowska H (2009) Influence of the precursor metamorphism degree on preparation of nitrogen-enriched activated carbons by ammoxidation and chemical activation of coals. *Energy Fuels* 23:2205–2212. <https://doi.org/10.1021/ef801094c>
66. Kruk M, Jaroniec M, Sayari (1997) A adsorption study of surface and structural properties of MCM-41 materials of different pore sizes. *J Phys Chem B* 101:583–589. <https://doi.org/10.1021/jp962000k>
67. Hwang J, Yoon D, Kweon B, Chang W, Kim J (2016) A simple, one-pot synthesis of molybdenum oxide-reduced graphene oxide composites in supercritical methanol and their electrochemical performance. *RSC Adv* 6:108298–108309. <https://doi.org/10.1039/C6RA24632J>
68. Qin J, Zhao N, Shi C, Liu E, He F, Ma L, Li Q, Li J, He C (2017) Sandwiched C@SnO₂@C hollow nanostructures as an ultralong-lifespan high-rate anode material for lithium-ion and sodium-ion batteries. *J Mater Chem A* 5:10946–10956. <https://doi.org/10.1039/C7TA01936J>
69. Yang LC, Sun W, Zhong ZW, Liu JW, Gao QS, Hu RZ, Zhu M (2016) Hierarchical MoO₃/N-doped carbon heteronanowires with high rate and improved long-term performance for lithium-ion batteries. *J Power Sources* 306:78–84. <https://doi.org/10.1016/j.jpowsour.2015.11.073>
70. Chen JS, Lou XW (2013) SnO₂-based nanomaterials: synthesis and application in lithium-ion batteries. *Small* 9:1877–1893. <https://doi.org/10.1002/smll.201202601>
71. Lou XW, Deng D, Lee JY, Archer LA (2008) Preparation of SnO₂/carbon composite hollow spheres and their lithium storage properties. *Chem Mater* 20:6562–6566. <https://doi.org/10.1021/cm801607e>
72. Zhang J, Huang T, Zhang L, Yu A (2014) Molybdenum-doped titanium dioxide and its superior lithium storage performance. *J Phys Chem C* 118:25300–25309. <https://doi.org/10.1021/jp506401q>
73. Stephenson T, Li Z, Olsen B, Mitlin D (2014) Lithium ion battery applications of molybdenum disulfide (MoS₂) nanocomposites. *Energy Environ Sci* 7:209–231. <https://doi.org/10.1039/C3EE42591F>
74. Luo W, Hu X, Sun Y, Huang Y (2011) Electrospinning of carbon-coated MoO₂ nanofibers with enhanced lithium-storage properties. *Phys Chem Chem Phys* 13:16735–16740. <https://doi.org/10.1039/C1CP22184A>
75. Sun Y, Hu X, Luo W, Huang Y (2012) Ultrafine MoO₂ nanoparticles embedded in a carbon matrix as a high-capacity and long-life anode for lithium-ion batteries. *J Mater Chem* 22:425–431. <https://doi.org/10.1039/C1JM14701C>
76. Zhang X, Huang X, Zhang X, Xia L, Zhong B, Zhang T, Wen G (2017) Cotton/RGO/carbon-coated SnO₂ nanoparticle-composites as superior anode for lithium ion battery. *Mater Design* 114:234–242. <https://doi.org/10.1016/728j.matdes.2016.11.081>

Publisher's note Springer Nature remains neutral with regard to jurisdictional claims in published maps and institutional affiliations.

Springer Nature or its licensor holds exclusive rights to this article under a publishing agreement with the author(s) or other rightsholder(s); author self-archiving of the accepted manuscript version of this article is solely governed by the terms of such publishing agreement and applicable law.